Catalysis Letters Vol. 112, Nos. 1–2, November 2006 (© 2006)
DOI: 10.1007/s10562-006-0158-z

Methane oxidation over nanocrystalline $Ce_{0.45}Zr_{0.45}La_{0.10}O_{2-\delta}$/Pt and $Ce_{0.9}Sm_{0.1}O_{2-\delta}$/Pt anodes

A. A. Yaremchenko,[a] V. V. Kharton,[a,b,*] A. A. Valente,[c] E. V. Frolova,[b] M. I. Ivanovskaya,[b] A. V. Kovalevsky,[a] F. M. B. Marques,[a] and J. Rocha[c]

[a]*Department of Ceramics and Glass Engineering, CICECO, University of Aveiro, Aveiro 3810-193, Portugal*
[b]*Institute of Physicochemical Problems, Belarus State University, 14 Leningradskaya Str., Minsk 220050, Belarus*
[c]*Department of Chemistry, CICECO, University of Aveiro, Aveiro 3810-193, Portugal*

Received 19 June 2006; accepted 8 September 2006

The electrocatalytic activity of composite anodes, comprising metallic platinum and nanocrystalline Pt-modified $Ce_{0.45}Zr_{0.45}La_{0.10}O_{2-\delta}$ and $Ce_{0.9}Sm_{0.1}O_{2-\delta}$, was evaluated for the oxidation of dry methane in a solid oxide fuel cell (SOFC) – type reactor with yttria-stabilized zirconia solid electrolyte. At 923–1073 K, the total combustion is dominant, whilst above 1100 K the composite anodes exhibit significant catalytic activity towards the partial oxidation of methane (POM). At 1223 K and for a O_2:CH_4 ratio equal to 0.5, stoichiometric for the POM reaction, CO selectivity and CH_4 conversion over $Ce_{0.9}Sm_{0.1}O_{2-\delta}$ /Pt achieves 55% and 41%, respectively. Under these conditions, $Ce_{0.45}Zr_{0.45}La_{0.10}O_{2-\delta}$ /Pt anodes possess higher catalytic activity for partial oxidation, associated with the lower lattice oxygen mobility and instability of the $Ce_{0.45}Zr_{0.45}La_{0.10}O_{2-\delta}$ cubic fluorite structure, and provide 54% conversion efficiency with 73% selectivity to carbon monoxide. Further increase in CH_4 conversion and CO selectivity can be achieved by packing the reactor with an additional catalyst, such as Pt-promoted $Ce_{0.45}Zr_{0.45}La_{0.10}O_{2-\delta}$ or $LaNiO_{3-\delta}/Al_2O_3$.

KEY WORDS: ceria; partial oxidation; methane; synthesis gas; SOFC anode.

1. Introduction

Solid oxide fuel cells (SOFCs) are considered as alternative electric power generation systems due to high fuel conversion efficiency, low pollutant emissions, low noise and fuel flexibility [1–4]. The direct oxidation of methane in SOFCs makes it possible to increase the open-circuit voltage, to eliminate reformer, and to co-generate electrical power and useful products such as synthesis gas, a mixture of CO and H_2 used as a feed-stock for the commercial methanol and Fischer–Tropsch synthesis. Recently, significant attention was drawn to Ce-containing oxide phases as components of anodes for hydrocarbon-fueled SOFCs [5–12]. Ceria and its derivatives, exhibiting mixed oxygen-ionic and electronic conductivity under reducing conditions, provide an enlargement of the electrochemical reaction zone, reduction of anode polarization [6,10–13], and continuous removal of carbon deposits due to oxygen storage/release capacity [5,6,14]. In addition, ceria-based materials show substantial catalytic activity for partial oxidation of methane (POM), $\frac{1}{2}O_2 + CH_4 \Rightarrow CO + 2H_2$ [14–19]. These components may, hence, promote selective electrochemical oxidation of methane directly on the SOFC anode $(O^{2-} + CH_4 \Rightarrow CO + 2H_2 + 2e^-)$.

*To whom correspondence should be addressed.
E-mail: kharton@cv.ua.pt

The present work is focused on the study of dry methane oxidation over SOFC anodes comprising Pt-modified nanocrystalline $Ce_{0.45}Zr_{0.45}La_{0.10}O_{2-\delta}$ and $Ce_{0.9}Sm_{0.1}O_{2-\delta}$. These ceria-based solid solutions were reported to exhibit significant catalytic activity for the oxidation of methane to synthesis gas by lattice oxygen [18,19]. Their catalytic activity can be further improved by modification of the surface with dispersed platinum, promoting methane dissociation and activation of lattice oxygen ions near the surface [18,19]. The n-type electronic conductivity of reduced ceria is however insufficient, which requires to incorporate another electronically-conducting component, preferably with a high catalytic activity. This combination of properties is characteristic of several transition metals (e.g. Ni) or noble metals (e.g. Pt). In the present work, platinum was selected as the second component of the model composite anodes, in order to avoid possible solid-state reactions with oxide components and prolonged relaxation processes typical for Ni-containing anodes on redox cycling.

2. Experimental

The nanocrystalline powders of $Ce_{0.45}Zr_{0.45}La_{0.10}O_{2-\delta}$ and $Ce_{0.9}Sm_{0.1}O_{2-\delta}$ were prepared by co-precipitation of metal hydroxides from the solution of

Ce^{3+}, ZrO^{2+} and La^{3+}, or Ce^{3+} and Sm^{3+} nitrates, containing metal cations in the stoichiometric proportions. The co-precipitation was performed adding aqueous ammonia under continuous stirring. After washing, the precipitates were peptized to a sol by a short (<1 min) ultrasonic treatment, dried in air, and then annealed at 873–1473 K. The characterization of powders included X-ray diffraction (XRD) analysis using HZC 4A and Rigaku D/MAX-B instruments, transmission electron microscopy (TEM, LEO 906E microscope), and scanning electron microscopy (SEM, Hitachi S-4100 microscope).

Studies of the electrocatalytic activity of $Ce_{0.45}Zr_{0.45}La_{0.10}O_{2-\delta}$ /Pt and $Ce_{0.9}Sm_{0.1}O_{2-\delta}$ /Pt composite anodes were carried out using a SOFC-type reactor with 8 mol.% yttria-stabilized zirconia (YSZ) solid electrolyte (figure 1(a)). The model SOFC-type reactor comprised one hermetically-sealed YSZ tube (inner diameter 8.9 mm, wall thickness 2.0 mm) with the composite anode applied onto the inner surface, and a Pt cathode on the outer surface. Pt wires were used as current collectors. As the current collectors were completely covered with anode material and their geometrical surface area was considerably smaller compared to anode layers (<0.1%), the influence of Pt wires on the catalytic performance of the reactor was considered negligible. For the fabrication of anodes, $Ce_{0.45}Zr_{0.45}La_{0.10}O_{2-\delta}$ and $Ce_{0.9}Sm_{0.1}O_{2-\delta}$ powders annealed at 873 K for 1 h were impregnated with H_2PtCl_6 solution (Pt loading of 1.5 wt.%) and dried at 373 K. Pt-modified $Ce_{0.45}Zr_{0.45}La_{0.10}O_{2-\delta}$ powder was grinded, mixed with coarse metallic Pt (50:50 wt.%), and applied onto YSZ surface with annealing at 1373 K for 1 h. The sheet density of $Ce_{0.45}Zr_{0.45}La_{0.10}O_{2-\delta}$ /Pt composite anodes was 6.7 $\pm$ 0.2 mg/cm^2. In the case of Sm-doped ceria, anodes were prepared in two steps applying metallic Pt porous layer on the YSZ surface (annealing at 1223 K for 0.5 h; sheet density 4.9 $\pm$ 0.1 mg/cm^2), and then Pt-modified $Ce_{0.9}Sm_{0.1}O_{2-\delta}$ powder over platinum layer (annealing at 1373 K for 1 h, sheet density 29 $\pm$ 1 mg/cm^2). Porous platinum anodes studied for comparison were prepared via similar procedure with annealing at 1223 K for 0.5 h. In all cases, geometric surface area of the composite anodes was 12.6 $\pm$ 0.3 cm^2.

In the course of experiments, a mixture of dry methane (≥99.995 % purity) and He (50:50 vol.%) was supplied onto the composite anodes with a total flow rate of 2–3 cm^3/min; the gas flow composition and rate were fixed by Bronkhorst mass-flow controllers. The influent flow rate was limited by the maximum current density through the solid-electrolyte membrane, determined by the ohmic and polarization resistances of the model SOFC-type reactor; in this work focused on the catalytic studies, the reactor was not optimized to decrease voltage losses. Oxygen was supplied into the reaction zone by passing direct current through the cell in the galvanostatic mode; the current density varied in the range 2.7–16.5 mA/cm^2, which corresponds to effective O_2:CH_4 ratios ranging from approximately 0.125 to 0.625. The experiments were performed in the temperature range from 973 to 1173 K. The composition of gas mixtures at the inlet and outlet of the reactor were analyzed using a Varian CP-3800 gas chromatograph, equipped with thermal-conductivity and flame-ionization detectors coupled in series and a 250 μl six-port VICI gas-sampling valve; the separation and quantification of gas components was accomplished

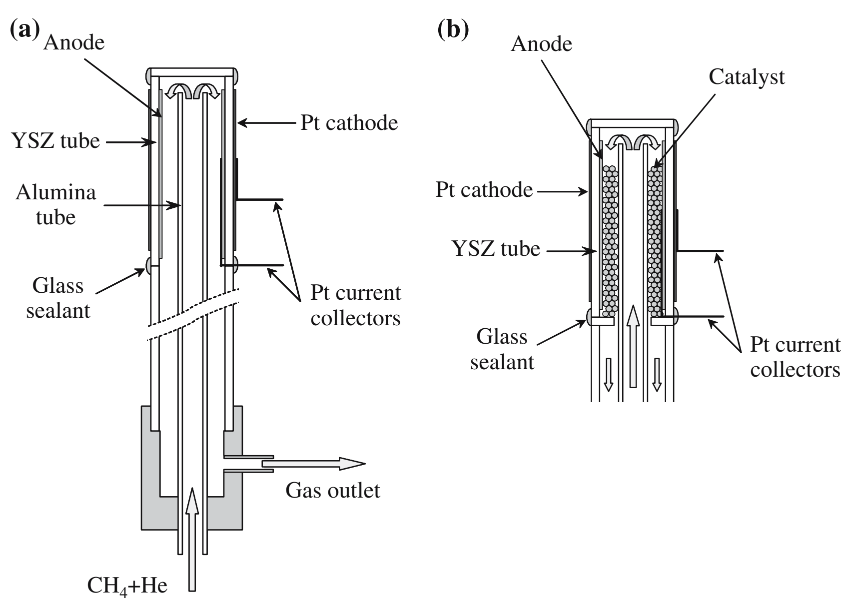

Figure 1. Schematic drawing of the model SOFC-type reactor for CH_4 oxidation (a) and upper part of the reactor packed with an additional catalyst (b).

with a semi-capillary CarboPLOT P7 column using the absolute calibration method. Analysis was performed as a function of time for at least 20 h for every set of conditions (at fixed temperature and O_2:CH_4 ratio). The product selectivity was calculated as the concentration ratio between a given product and the sum of all detected carbon-containing products, namely CO, CO_2, C_2H_6 , C_2H_4 and C_2H_2 . The selectivity to C_2 hydrocarbons was below 1.5%. The yield of carbon monoxide was calculated as the ratio between outlet CO and inlet CH_4 flow rates.

In selected cases, the SOFC-type reactor was packed with an additional catalyst, namely, Pt-modified $Ce_{0.45}Zr_{0.45}La_{0.10}O_{2-\delta}$ or $Pt/LaNiO_3/Al_2O_3$, as illustrated in figure 1(b). For the preparation of $Pt/LaNiO_3/Al_2O_3$ catalyst, porous Al_2O_3 spheres (diameter 1.5–2.0 mm, surface area 200 m^2/g) were impregnated with aqueous solution of lanthanum and nickel nitrates, containing metal cations in equimolar proportion, and then annealed at 773 K for 2 h in air to form $LaNiO_3$. The resultant $LaNiO_3$ loading was 14.5 % with respect to Al_2O_3 weight. Further, the spheres were impregnated with H_2PtCl_6 solution in ethanol (Pt loading 2.0 wt.% with respect to $LaNiO_3$) and annealed again at 773 K for 2 h.

3. Results and discussion

XRD showed partial crystallization of $Ce_{0.45}Zr_{0.45}La_{0.10}O_{2-\delta}$ and $Ce_{0.9}Sm_{0.1}O_{2-\delta}$ powders annealed at 873–1373 K (figure 2). All reflections can be assigned to a cubic fluorite-type phase, space group $Fm\overline{3}m$. The XRD patterns are broadened due to nanoscale particle size; the average crystalline size calculated by the Scherer equation was in the range of 4–5 nm and 8–10 nm for powders annealed at 873 K and 1373 K, respectively. Note that the formation of several metastable phases was observed in the intermediate region (ceria content 20–80 mol.%) of the $CeO_2 - ZrO_2$ phase diagram [20]; $Ce_{0.5}Zr_{0.5}O_{2-\delta}$ solid solution undergoes phase separation to thermodynamically stable cubic Ce-rich and tetragonal Zr-rich solid solutions on thermal treatment [21]. Also, segregation of two fluorite-type solid solutions was reported for $(Ce_{0.5}Zr_{0.5})_{1-x}La_xO_{2-\delta}$ with x ≥ 0.2 [18]. In combination with these data, the XRD results suggest formation of a metastable solid solution for the $Ce_{0.45}Zr_{0.45}La_{0.10}O_{2-\delta}$ composition.

The average particle size, estimated from the TEM results (figure 3(a)), is 3–5 nm and 8–12 nm for the powders annealed at 873 K and 1373 K, respectively, in excellent agreement with the XRD data. Increasing the temperature of treatment to 1473 K promotes further crystallization (figure 2) and grain growth (figure 3(b)), although after 10 h a fraction of nano-sized particles is still kept (inset in figure 3(b)). The sintering of $Ce_{0.45}Zr_{0.45}La_{0.10}O_{2-\delta}$ /Pt and $Ce_{0.9}Sm_{0.1}O_{2-\delta}$ /Pt anodes as well as the final pre-treatment of the Pt-

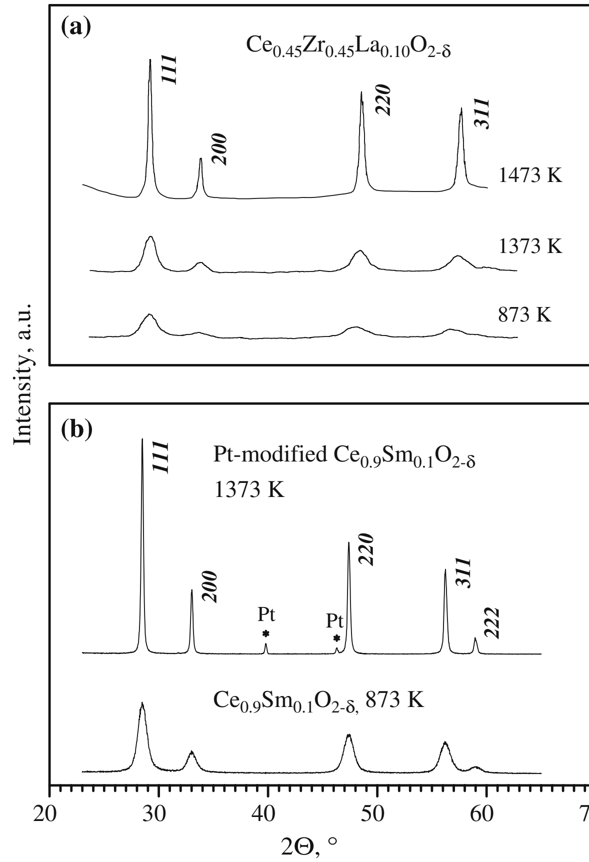

Figure 2. XRD patterns of $Ce_{0.45}Zr_{0.45}La_{0.10}O_{2-\delta}$ (a), $Ce_{0.9}Sm_{0.1}O_{2-\delta}$ and Pt-modified $Ce_{0.9}Sm_{0.1}O_{2-\delta}$ (b) powders annealed at 873–1373 K for 1 h or at 1473 K for 10 h. The *hkl* indexes are given for the cubic fluorite-type structure (space group $Fm\overline{3}m$).

modified $Ce_{0.45}Zr_{0.45}La_{0.10}O_{2-\delta}$ catalyst packed into the model reactor were thus performed at 1373 K for 1 h. Both catalyst and anodes consisted of aggregates formed by Pt-modified $Ce_{0.45}Zr_{0.45}La_{0.10}O_{2-\delta}$ or $Ce_{0.9}Sm_{0.1}O_{2-\delta}$ nanocrystallites, figure 3(C–E) and figure 4; large Pt particles formed a continuous network providing current collection.

The conversion of dry methane over $Ce_{0.45}Zr_{0.45}La_{0.10}O_{2-\delta}$ /Pt anodes at 973–1073 K results in dominant CO_2 formation even at low O_2:CH_4 ratio (figure 5). Increasing temperature to 1173 K leads to a sharp increase of the catalytic activity towards partial oxidation reaction (figures 5 and 6). For the effective O_2:CH_4 ratio of 0.5, stoichiometric for the POM, CH_4 conversion and selectivity to carbon monoxide achieves 54% and 73%, respectively. Note that this ratio, calculated from the oxygen flux through solid-electrolyte membrane, reflects only the total concentration of oxygen atoms in the gaseous phase; the methane oxidation is expected to occur both electrochemically and via the chemical reactions with oxygen atoms or molecules formed due to discharge of O^{2-} anions. At the same time, no gaseous O_2 was detected in the effluent gas

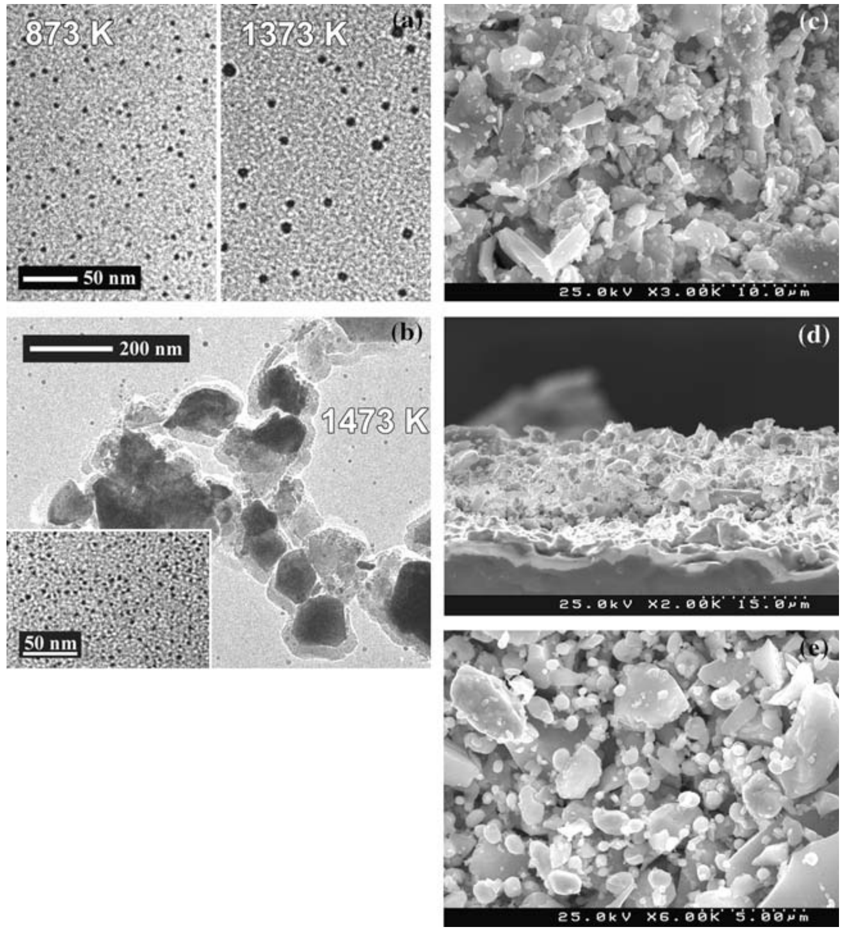

Figure 3. Bright-field TEM (a,b) and SEM (c–e) images of $Ce_{0.45}Zr_{0.45}La_{0.10}O_{2-\delta}$ powders annealed at 873 K and 1373 K for 1 h (a), $Ce_{0.45}Zr_{0.45}La_{0.10}O_{2-\delta}$ powder annealed at 1473 K for 10 h (b), Pt-modified $Ce_{0.45}Zr_{0.45}La_{0.10}O_{2-\delta}$ catalyst (c), and $Ce_{0.45}Zr_{0.45}La_{0.10}O_{2-\delta}$ /Pt anode on YSZ solid electrolyte (d and e).

mixtures, suggesting that the oxidation processes are localized mainly at the electrode surface.

Under similar conditions (O_2:CH_4 = 0.5, 1223 K), methane oxidation over porous Pt anode results in lower conversion but higher selectivity to CO (figure 6), which may indicate a contribution of the reverse water-gas shift reaction. The practical use of platinum anodes is, however, impossible due to extensive carbon deposition; coking limited the operation of these anodes to 35–40 h even at a O_2:CH_4 ratio close to 0.5. On the contrary, no carbon imbalance between the influent and effluent gas mixtures was observed for $Ce_{0.45}Zr_{0.45}La_{0.10}O_{2-\delta}$ /Pt composite anodes within the limits of experimental uncertainty ($\pm 5\%$) when the oxygen-to-methane ratio was above 0.37.

Further improvement in the reactor performance was achieved by packing with Pt-modified $Ce_{0.45}Zr_{0.45}La_{0.10}O_{2-\delta}$ catalyst (2.3 g) as illustrated by figure 1(b). Incorporation of additional catalyst has a rather small effect at 923–1073 K, but increases conversion efficiency approximately twice and also improves selectivity to carbon monoxide at 1123–1173 K (figures 5 and 6). Both CH_4 conversion and CO selectivity approach the theoretical equilibrium values, calculated assuming negligible carbon formation, and achieve 87% and 84%, respectively, at 1173 K and O_2:CH_4 ratio of 0.5 (figure 6). Such an improvement is due to reforming of residual methane on the catalyst surface with H_2O and CO_2 formed at the anode:

$$CH_4 + H_2O \Rightarrow CO + 3H_2$$

$$CH_4 + CO_2 \Rightarrow 2CO + 2H_2$$

Consequently, the outlet mixture composition becomes closer to the thermodynamically predicted values. The performance of the reactor with $Ce_{0.45}Zr_{0.45}La_{0.10}O_{2-\delta}$ / Pt anode and Pt-modified $Ce_{0.45}Zr_{0.45}La_{0.10}O_{2-\delta}$ catalyst was found stable with no evidence of degradation with time at 1173 K (figure 7).

The results show that Pt-modified $Ce_{0.45}Zr_{0.45}La_{0.10}O_{2-\delta}$ exhibits a high catalytic activity towards POM and is effective enough in preventing carbon deposition at the SOFC-type reactor anode. At the same type, deep microstructural optimization of

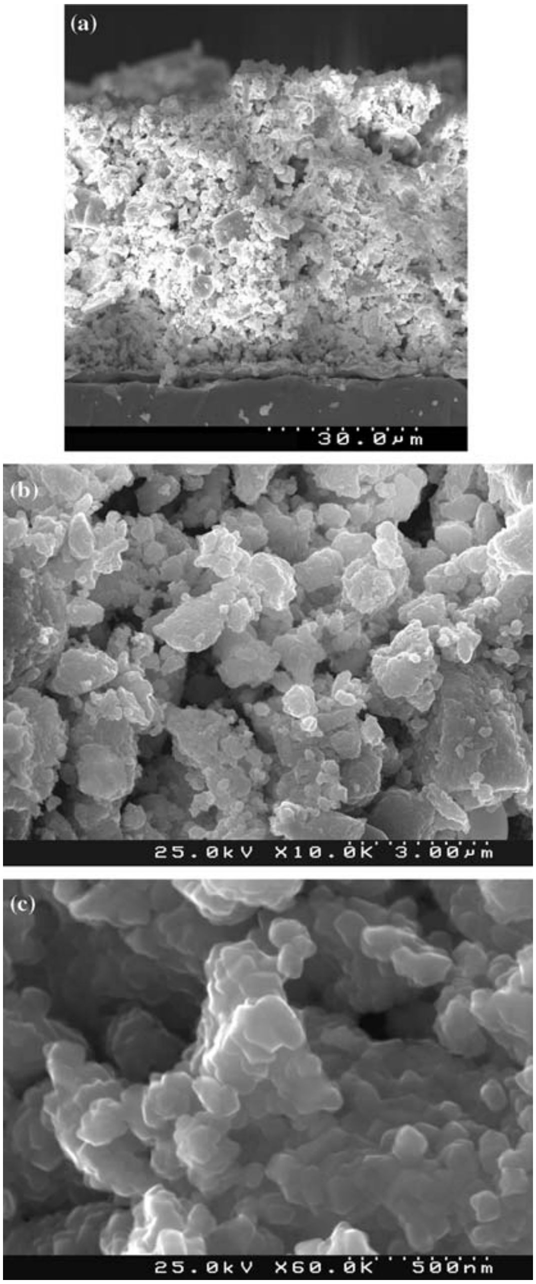

Figure 4. SEM images of $Ce_{0.9}Sm_{0.1}O_{2-\delta}$ /Pt anode on YSZ solid electrolyte: cross-section (a) and surface (b and c).

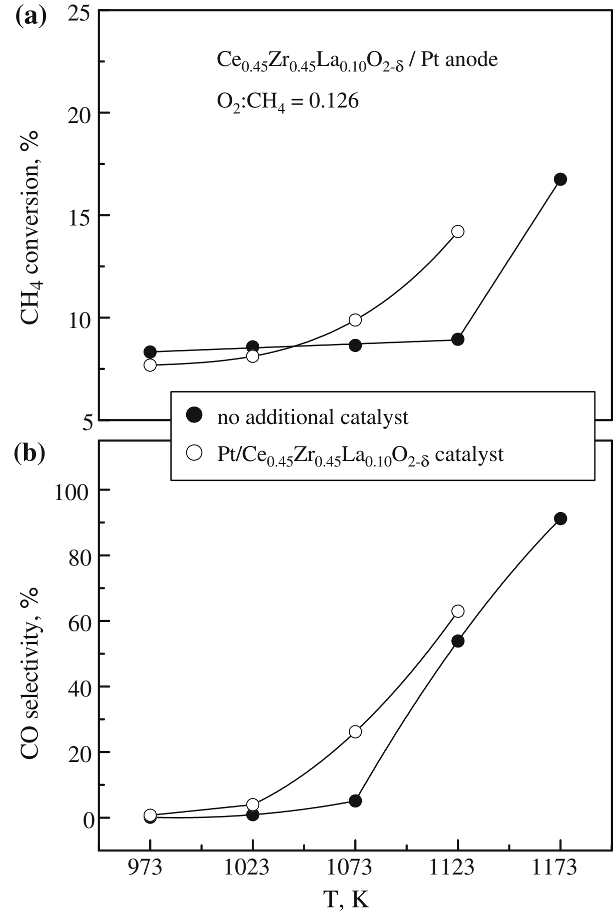

Figure 5. Temperature dependence of the methane conversion (a) and selectivity to CO formation (b) in SOFC-type reactor with $Ce_{0.45}Zr_{0.45}La_{0.10}O_{2-\delta}$ /Pt anode.

$Ce_{0.45}Zr_{0.45}La_{0.10}O_{2-\delta}$ - containing anodes is necessary in order to achieve CO yields close to theoretical values without the use of an additional reforming catalyst. The conversion of methane to synthesis gas occurs typically via a two-stage mechanism, which involves the total combustion of CH_4 and subsequent reforming of remaining methane with CO_2 and H_2O [22]. When the reactor is not packed with extra catalyst, the presence of significant fractions of CO_2 in the outlet mixture is associated with incomplete reforming at the anode.

As for $Ce_{0.45}Zr_{0.45}La_{0.10}O_2$ -containing electrodes, methane oxidation over $Ce_{0.9}Sm_{0.1}O_{2-\delta}$ /Pt anodes results in total combustion at 973–1073 K (figure 8). At a $O_2 : CH_4$ ratio of 0.5, the selectivity to CO did not exceeded 1.3% with a 27% conversion efficiency. Increasing temperature to 1173 K improved the electrocatalytic performance; CH_4 conversion and CO selectivity achieve 41% and 55%, respectively. The conversion and selectivity to carbon monoxide are, however, lower compared to $Ce_{0.45}Zr_{0.45}La_{0.10}O_{2-\delta}$ /Pt cermets and porous Pt anodes under similar conditions (figure 6).

The difference in the catalytic behavior of $Ce_{0.45}Zr_{0.45}La_{0.10}O_{2-\delta}$ and $Ce_{0.9}Sm_{0.1}O_{2-\delta}$ can be related to two major factors, namely lattice oxygen mobility and metastability of the $Ce_{0.45}Zr_{0.45}La_{0.10}O_{2-\delta}$ fluorite-type structure. The mobility of oxygen ions in the ceria lattice may play an important role in the catalytic performance influencing oxygen supply from the bulk to active surface centers and the kinetics of redox process. For instance, an inverse correlation between lattice oxygen mobility and selectivity towards POM was observed for $Ce_{1-x}Gd_xO_{2-\delta}$ fluorite-type solid solutions [23]. Higher oxygen mobility in $Ce_{0.9}Sm_{0.1}O_{2-\delta}$ compared to that in $Ce_{0.45}Zr_{0.45}La_{0.10}O_{2-\delta}$ [19] should

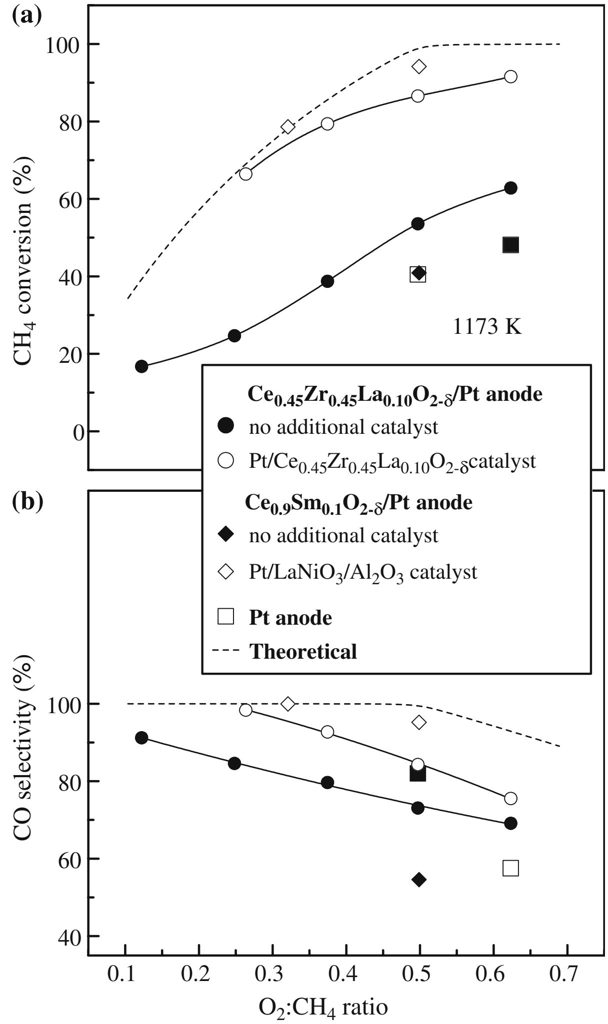

Figure 6. Dependence of CH_4 conversion (a) and CO selectivity (b) on the effective $O_2 : CH_4$ ratio in SOFC-type reactors with $Ce_{0.45}Zr_{0.45}La_{0.10}O_{2-\delta}$ /Pt and $Ce_{0.9}Sm_{0.1}O_{2-\delta}$ /Pt anodes.

promote the activation of oxygen ions at the platinum/oxide interface and result in faster oxidation of methane and/or partial oxidation products. On the other hand,

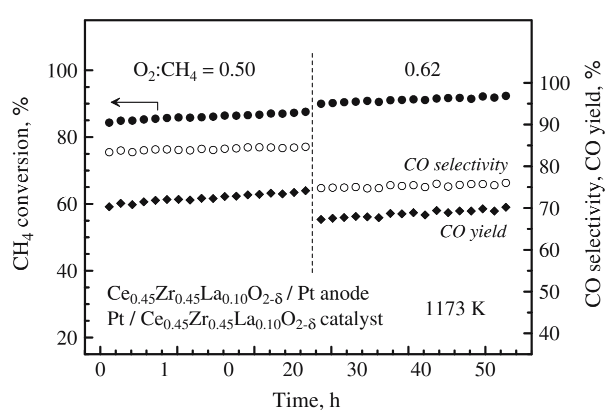

Figure 7. Example of time dependence of methane conversion, CO selectivity and CO yield over $Ce_{0.45}Zr_{0.45}La_{0.10}O_{2-\delta}$ /Pt anode in the reactor packed with additional $Pt/Ce_{0.45}Zr_{0.45}La_{0.10}O_{3-\delta}$ catalyst.

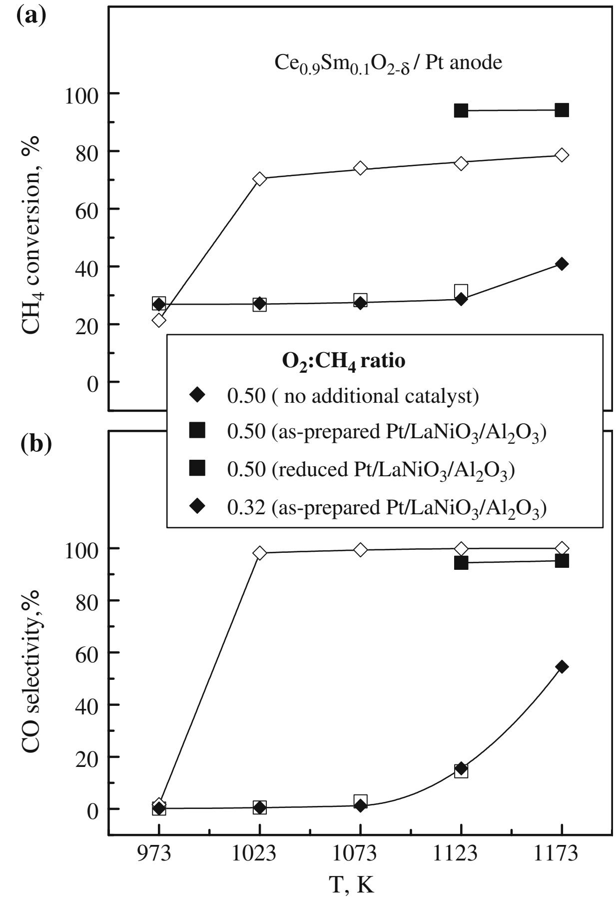

Figure 8. Temperature dependence of the methane conversion (a) and selectivity to CO formation (b) in SOFC-type reactor with $Ce_{0.9}Sm_{0.1}O_{2-\delta}$ /Pt anode.

the instability of the $Ce_{0.45}Zr_{0.45}La_{0.10}O_{2-\delta}$ cubic lattice, especially in the surface layers, is expected to increase the concentration of surface defects / active centers, thus improving the catalytic activity.

Since the catalytic performance of Pt-modified $Ce_{0.9}Sm_{0.1}O_{2-\delta}$ for POM reaction was rather insufficient, the model SOFC-type reactor with $Ce_{0.9}Sm_{0.1}O_{2-\delta}$ /Pt anodes was packed with $Pt/LaNiO_3/Al_2O_3$ catalyst (1.5 g). $LaNiO_3$ is a well-established catalyst precursor for methane conversion processes, which transforms into Ni^0/La_2O_3 in reducing environments [24,25]. Reduction of $LaNiO_3$ results in a fine dispersion of nickel metal particles over porous lanthanum oxide, thus limiting the coke formation characteristic for nickel catalysts [25,26].

Packing the reactor with $Pt/LaNiO_3/Al_2O_3$ apparently did not result in any improvement in catalytic performance at 973–1123 K with effective $O_2 : CH_4$ ratio of 0.5 (figure 8). This indicates that the oxygen chemical potential in the reactor under these conditions was higher than required to activate $LaNiO_{3-\delta}$ precursor. The $O_2 : CH_4$ ratio was hence decreased down to $\sim$0.16 and the catalyst precursor was reduced in methane-rich conditions at 1123 K for several hours, as illustrated by figure 9; then the oxygen-to-methane ratio of 0.5 was restored. The reduction results in a drastic increase of methane conversion from 32 to 94% and CO selectivity from 14 to 94% at 1173 K (figures 8 and 9). At a lower O_2:CH_4 ratio of 0.32, the reduction of catalyst occurs on heating from 973 to 1023 K without additional treatment, providing 98.2–99.9% CO selectivity at 1023–1173 K (figure 8). The operation under oxygen-lean conditions results, however, in incomplete methane conversion and increases the risks of rapid deactivation of the catalyst due to coking. When the oxygen-to-methane ratio is stoichiometric for POM, the conversion efficiency and CO selectivity at 1173 K achieves 94.2% and 95.2%, respectively, being slightly below thermodynamic equilibrium values (figure 6). The reactor performance was found stable, with no evidence of time degradation (figure 10) or carbon imbalance between influent and effluent gas compositions within the limits of experimental error, although minor traces of carbon deposits on the catalyst surface were detected by temperature-programmed oxidation after operation at 1123–1173 K for 60 h.

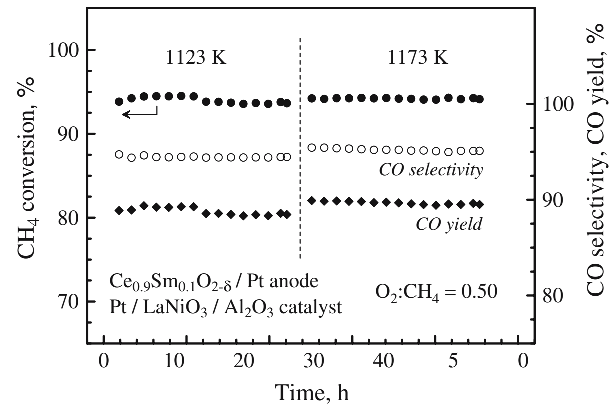

Figure 10. Time dependence of methane conversion, CO selectivity and CO yield over $Ce_{0.9}Sm_{0.1}O_{2-\delta}$ /Pt anode in the reactor packed with additional Pt/$LaNiO_3$/Al_2O_3 catalyst.

4. Conclusions

Dry methane oxidation over composite anodes, consisting of metallic platinum and platinum-promoted nanocrystalline $Ce_{0.45}Zr_{0.45}La_{0.10}O_{2-\delta}$ and $Ce_{0.9}Sm_{0.1}O_{2-\delta}$ prepared by an organic-free sol-gel method, was studied using a model SOFC-type reactor with YSZ solid electrolyte. Methane conversion over composite anodes results in dominant total oxidation at 973–1073 K. Increasing temperature above 1100 K leads to a significant increase of catalytic activity towards POM. For the O_2 to CH_4 ratio of 0.5, stoichiometric for the partial oxidation reaction, CO selectivity and methane conversion over $Ce_{0.45}Zr_{0.45}La_{0.10}O_{2-\delta}$ /Pt anodes achieves 73% and 54%, respectively, at 1223 K. Packing with additional Pt-modified nanocrystalline $Ce_{0.45}Zr_{0.45}La_{0.10}O_{2-\delta}$ catalyst results in further improvement of the model reactor performance and provides 84% CO selectivity with 87% conversion efficiency. This confirms the high activity of Pt-modified $Ce_{0.45}Zr_{0.45}La_{0.10}O_{2-\delta}$ for the partial oxidation of methane and suggests a possibility for further microstructural optimization of $Ce_{0.45}Zr_{0.45}La_{0.10}O_{2-\delta}$ - containing anodes in order to achieve 95–97% CO yield, even without the use of an additional reforming catalyst.

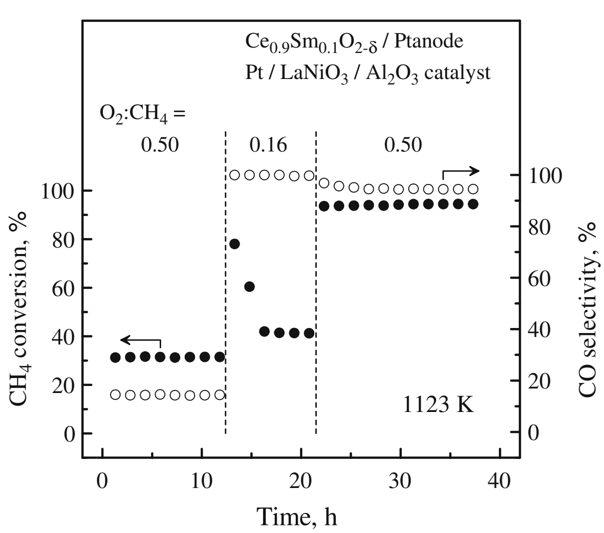

Figure 9. Time dependence of methane conversion and CO selectivity in the reactor with $Ce_{0.9}Sm_{0.1}O_{2-\delta}$ /Pt anode, illustrating the effect of reduction of Pt/$LaNiO_3$/Al_2O_3 catalyst at 1123 K.

$Ce_{0.9}Sm_{0.1}O_{2-\delta}$ /Pt anodes show a lower activity for the partial oxidation reaction. At 1223 K and O_2:CH_4 ratio equal to 0.5, the selectivity to carbon monoxide is 55% with 41% methane conversion. The difference in catalytic behavior of $Ce_{0.9}Sm_{0.1}O_{2-\delta}$ and $Ce_{0.45}Zr_{0.45}La_{0.10}O_{2-\delta}$ can be related to the lower lattice oxygen mobility and instability of the cubic fluorite lattice for the latter composition. On the other hand, high oxygen mobility in the $Ce_{0.9}Sm_{0.1}O_{2-\delta}$ lattice is expected to provide better resistance to carbon deposition. Significant improvement in methane conversion and CO selectivity, up to 94.2% and 95.2% respectively, can be achieved incorporating a Pt/$LaNiO_3$/Al_2O_3 catalyst into the reactor with $Ce_{0.9}Sm_{0.1}O_{2-\delta}$ /Pt composite anodes. Taking into account the tendency of nickel-based catalyst to deactivation by coking, the long-term tests are required to evaluate the stability of reactor performance.

Acknowledgments

This work was partially supported by the FCT, Portugal (project POCI/CTM/58570/2004 and SFRH/BPD/15003/2004), and by the NATO Science for Peace program (project 978002).

References

[1] R.M. Ormerod, Chem. Soc. Rev. 32 (2003) 17.
[2] N.Q. Minh, Solid State Ionics 174 (2004) 271.
[3] F. Alcaide, P.L. Cabot and E. Brillas, J. Power Sources 153 (2006) 47.
[4] M. Mogensen and K. Kammer, Annu. Rev. Mater. Res. 33 (2003) 321.
[5] B. Rösch, H. Tu, A.O. Störmer, A.C. Müller and U. Stimming, Solid State Ionics 175 (2004) 113.
[6] E.P. Murray, T. Tsai and S.A. Barnett, Nature 400 (1999) 649.
[7] A.A. Yaremchenko, A.A. Valente, V.V. Kharton, I.A. Bashmakov, J. Rocha and F.M.B. Marques, Catal. Comm. 4 (2003) 477.
[8] M. Itome and A.E. Nelson, Catal. Lett. 106 (2006) 21.
[9] S. Park, R.J. Gorte and J.M. Vohs, Appl. Catal. A 200 (2000) 55.
[10] J.B. Wang, J.-C. Jang and T.-J. Huang, J. Power Sources 122 (2003) 122.
[11] R.J. Gorte, H. Kim and J.M. Vohs, J. Power Sources 106 (2002) 10.
[12] E.V. Tsipis, V.V. Kharton, I.A. Bashmakov, E.N. Naumovich and J.R. Frade, J. Solid State Electrochem. 8 (2004) 674.
[13] V.V. Kharton, E.N. Naumovich, V.N. Tikhonovich, I.A. Bashmakov, L.S. Boginsky and A.V. Kovalevsky, J. Power Sources 79 (1999) 242.
[14] E. Ramírez-Cabrera, A. Atkinson and D. Chadwick, Appl. Catal. B 36 (2002) 193.
[15] P. Pantu and G.R. Gavalas, Appl. Catal. A 223 (2002) 253.
[16] T. Zhu and M. Flytzani-Stephanopoulos, Appl. Catal. A 208 (2001) 403.
[17] W. Wang, S.M. Stagg-Williams, F.B. Noronha, L.V. Mattos and F.B. Passos, Catal. Today 98 (2004) 553.
[18] T.G. Kuznetsova, V.A. Sadykov, S.A. Veniaminov, G.M. Alikina, E.M. Moroz, V.A. Rogov, O.N. Martyanov, V.F. Yudanov, I.S. Abornev and S. Neophytides, Catal. Today 91(-92) (2004) 161.
[19] V.A. Sadykov, T.G. Kuznetsova, G.M. Alikina, Y.V. Frolova, A.I. Lukashevich, Y.V. Potapova, V.S. Muzykantov, V.A. Rogov, V.V. Kriventsov, D.I. Kochubei, E.M. Moroz, D.I. Zyuzin, V.I. Zaikovskii, V.N. Kolomiichuk, E.A. Paukshtis, E.B. Burgina, V.V. Zyryanov, N.F. Uvarov, S. Neophytides and E. Kemnitz, Catal. Today 93–95 (2004) 45.
[20] R. Di Monte and J. Kašpar, J. Mater. Chem. 15 (2005) 633.
[21] G. Colón, F. Valdivieso, M. Pijolat, R.T. Baker, J.J. Calvino and S. Bernal, Catal. Today 50 (1999) 271.
[22] A.P.E. York, T. Xiao and M.L.H. Green, Top. Catal. 22 (2003) 345.
[23] V.A. Sadykov, Yu.V Frolova, G.M. Alikina, A.I. Lukashevich and S. Neophytides, React. Kinet. Catal. Lett. 85 (2005) 375.
[24] V.R. Choudhary, B.S. Uphade and A.A. Belhekar, J. Catal. 163 (1996) 312.
[25] C. Batiot-Dupeyrat, G.A.S. Gallego, F. Mondragon, J. Barrault and J.-M. TatibouëtCatal., Today 107–108 (2005) 474.
[26] C.H. Bartholomew, Catal. Rev. Sci. Eng. 24 (1982) 67.